applied optics

Theoretical and experimental investigation of singly resonant optical parametric oscillator under double-pass pumping

PENG LI, YUANJI LI, JINXIA FENG, AND KUANSHOU ZHANG*

State Key Laboratory of Quantum Optics and Quantum Optics Devices, Institute of Opto-Electronics, Shanxi University, Taiyuan 030006, China
*Corresponding author: kuanshou@sxu.edu.cn

Received 4 February 2015; revised 11 March 2015; accepted 15 March 2015; posted 16 March 2015 (Doc. ID 234012); published 5 May 2015

The singly resonant optical parametric oscillator (SRO) under double-pass pumping in a two-mirror linear cavity is investigated theoretically and experimentally. Different output couplers are used in the periodically poled lithium niobate based SRO to optimize the extracted signal output. When the 2.5% output coupler is used, a pump threshold as low as 3.7 W is achieved, and 6.2 W of signal at 1.56 μm with the linewidth of 62.5 kHz is obtained at pump power of 14.5 W. The measured signal frequency drift and peak-to-peak power fluctuation are less than ±40 MHz and ±0.9% in a given 1 h, respectively.

OCIS codes: (190.0190) Nonlinear optics; (190.4970) Parametric oscillators and amplifiers; (140.3570) Lasers, single-mode.

http://dx.doi.org/10.1364/AO.54.004374

1. INTRODUCTION

Continuous-wave (cw) optical parametric oscillators (OPOs) are outstanding sources of radiation in the near- to mid-infrared with the advantages of high power, narrow linewidth, broad wavelength tunability, which can be widely used in the fields of atomic physics [1], high-resolution spectroscopy [2], trace gas sensing [3], as well as quantum optics and quantum information processing. Particularly, continuous variable quantum key distribution [4,5] based on the quantum entanglement at 1.5–1.6 μm can extend the transmission distance since the optical field at this wavelength can transmit over the fiber with the lowest loss. Therefore, cw single-frequency lasers at 1.5–1.6 μm are required to produce the quantum entanglement at a telecommunication wavelength [6,7]. Compared with the cw single-frequency erbium fiber lasers that exist large excess noises [8] and laser-diode-pumped Er, Yb-codoped crystal lasers where the output power is limited owing to the poor optical quality and serious thermal effects of the laser medium [9,10], output-coupled singly resonant OPO (OC-SRO) is an available way to extract high output power, low noise, cw single-frequency lasers in the 1.5–1.6 μm wavelength range [11–14].

Optimization of output coupling is a critical issue for scaling the extracted resonant power in a cw OC-SRO. In 2011, Kumar *et al.* reported a fiber-laser-pumped cw OC-SRO providing 9.8 W of signal at 1.629 μm together with 7.7 W of idler at 3.067 μm with 34.2% signal extraction efficiency and pump threshold of 10.5 W using an optimal output coupling of ~3.8% [14]. In 2012, Pabœuf *et al.* optimized the output coupling of a 532 nm laser-pumped OC-SRO using an intracavity plate and obtained a power of 1.6 W at 1.2 μm with a pump depletion of 80% and pump threshold of 3.2 W [15]. Recently, Zeil *et al.* obtained 19 W of signal at 1.55 μm and 11 W of idler at 3.4 μm with 47.5% signal extraction efficiency and pump threshold of 16 W by employing a variable-reflectivity volume Bragg grating as the output coupler [11]. The ring configuration SRO provides better frequency stability and more space for intracavity elements than the linear cavity, but the pump threshold should be even higher in order to get high output power and the maximum pump depletion can be obtained when the pumping ratio (namely, the ratio of the pump power to the pump threshold power) of $(\pi/2)^2$ (roughly 2.5) is reached [16]. However, with such a high pump threshold, the SRO has to be pumped by a high-power pump source. In practice, the linear cavity provides advantages of simpler setup, easier to align, lower loss, and less sensitive to small misalignments [17,18]. Especially high output power can be achieved from a double-pass-pumping (DPP) linear cavity configuration SRO with a lower pump threshold. As theoretically predicted in a plane-wave approximation, a pump depletion of 100% can be obtained when the pumping ratio is $\pi^2/2$ (roughly 5) [19].

In this paper, we extend the theory of the single-pass-pumping (SPP) SRO to the DPP scheme at first, then we demonstrate a cw single-frequency 1.56 μm laser by a DPP-SRO based on a periodically poled lithium niobate (PPLN). By optimizing the signal output using different output couplers, the best SRO performance was achieved and the characteristics of

signal at 1.56 μm, such as output power, linewidth, frequency and power stabilities, were investigated in detail.

2. THEORETICAL DESCRIPTION

In order to give a guideline for the design and optimization of the DPP-SRO with only signal resonated in the cavity, we extend the Guha's theory of SPP-SRO [20] to the DPP scheme. Here, the collimated Gaussian beam approximation is adopted, since the focusing parameters of pump and signal were selected to be nearly one in our experiments, i.e., the crystal is located at the Rayleigh length of the cavity modes. Meanwhile, the phase mismatch and thermal effects induced by the absorptions are ignored for simplicity.

Figure 1 shows the schematic of the DPP-SRO to be investigated in our experiment. The pump wave (ω_p) is injected into the cavity through the input coupler that is high transmission for pump. Then it propagates through the nonlinear crystal, in which the signal (ω_s) with power gain ΔP_s and idler (ω_i) are generated. Subsequently the residual pump wave is completely reflected back at the output coupler and passes through the crystal again, leading to another signal power gain $\Delta P_s'$. P_{rp} is the reflected pump power from the cavity. For the signal wave, the power reflection on the input coupler is assumed to be 100%, whereas the power transmission on the output coupler (T_s) is a variable to be optimized.

The signal power gain on the forward leg is given as [20]

$$\begin{aligned}\Delta P_s &= -8d\varepsilon_0\omega_s \,\mathrm{Im}\int A_s^* A_p A_i^* \mathrm{d}x\mathrm{d}y\mathrm{d}z \\ &= 8d\varepsilon_0\omega_s \int_0^\infty 2\pi r\mathrm{d}r \frac{q_1^*}{q} A_s^* |A_p(0)|^2 \\ &\quad \times \int_0^l \mathrm{d}z\, \sin(qz)\cos(qz), \end{aligned} \tag{1}$$

$$q_1 \equiv \frac{4\pi d}{\lambda_i n_i} A_s^*, \qquad q_2 \equiv \frac{4\pi d}{\lambda_p n_p} A_s, \qquad q \equiv \sqrt{q_1 q_2}, \tag{2}$$

where the subscripts p, s, and i denote the pump, signal, and idler fields, respectively. $A_{p,s,i}$ represent the corresponding amplitudes on the forward leg, $\lambda_{p,s,i}$ are the corresponding wavelengths in vacuum. $n_{p,s,i}$ denote the refractive indices of the crystal at the angular frequencies of $\omega_{p,s,i}$. d is the effective nonlinear coefficient of the crystal. ε_0 is the vacuum permittivity. l is the length of the crystal. P_p is the incident pump power. r and z are the transverse radial and longitudinal coordinates, respectively.

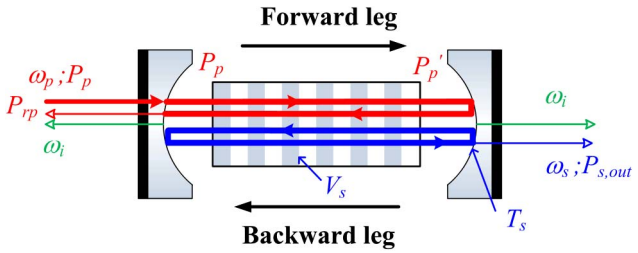

Fig. 1. Schematic of a DPP-SRO with only signal resonated.

To simplify the expression of ΔP_s in Eq. (1), the mode overlap between pump beam and signal mode (m) and the normalized parameter (u) are introduced:

$$\begin{aligned} m &= w_{0p}^2/w_{0s}^2; \\ u &= r^2/w_{0p}^2, \end{aligned} \tag{3}$$

where w_{0p} and w_{0s} are the waist radii of focused pump beam and signal mode, respectively. ΔP_s can be rewritten as

$$\Delta P_s = \frac{2\lambda_p}{\lambda_s} P_p \int_0^\infty \exp(-2u)\sin^2[gl\,\exp(-mu)]\mathrm{d}u. \tag{4}$$

g is defined by

$$g^2 l^2 = \frac{32\pi^2 d^2 l \xi_s P_s}{n_p n_s \lambda_i^2 \lambda_p c\varepsilon_0 (k-1)}, \tag{5}$$

where P_s is the intracavity signal power, k is defined as k_p/k_s. The wave vector $k_{p,s,i} = 2\pi n_{p,s,i}/\lambda_{p,s,i}$, and the focus factor $\xi_{p,s} = l/(k_{p,s} w_{0p,s}^2)$. c is the vacuum light speed.

Then the pump power at the end of the nonlinear crystal on the forward leg can be read as

$$\begin{aligned} P_p' &= \left(P_p - \Delta P_s \frac{\lambda_s}{\lambda_p}\right) \\ &= P_p\left\{1 - 2\int_0^\infty \exp(-2u)\sin^2[gl\,\exp(mu)]\mathrm{d}u\right\}. \end{aligned} \tag{6}$$

Similarly, the gain of signal power on the backward leg can be given as follows:

$$\begin{aligned} \Delta P_s' &= -8d\varepsilon_0\omega_s \,\mathrm{Im}\int A_s'^* A_p' A_i'^* \mathrm{d}x'\mathrm{d}y'\mathrm{d}z' \\ &= 8d\varepsilon_0\omega_s \int_0^\infty 2\pi r'\mathrm{d}r' \frac{q_1^*}{q} A_s^* |A_p'(0)|^2 \\ &\quad \times \int_0^l \mathrm{d}z'\, \sin(qz')\cos(qz') \\ &= \frac{2\lambda_p}{\lambda_s} P_p' \int_0^\infty \exp(-2u')\sin^2[gl\,\exp(-mu')]\mathrm{d}u', \end{aligned} \tag{7}$$

where z' is the new coordinate axis along the backward direction, and $z' = 0$ indicate the end of the crystal on the forward leg. $A_{p,s,i}'$ represent the amplitudes of the pump, signal, and idler fields on the backward leg, respectively.

When the DPP-SRO is operated stably, the oscillation condition is

$$\Delta P_s + \Delta P_s' = P_s(T_s + V_s), \tag{8}$$

where V_s denotes the absorptive and other losses for the resonant signal in the cavity.

By using Eqs. (2) and (5), and substituting Eqs. (4), (6), and (7) into Eq. (8), P_s can be obtained as an implicit function of P_p. The extracted signal power from the DPP-SRO and the threshold power are given by

$$P_{s,\mathrm{out}} = T_s P_s, \tag{9}$$

$$P_{\mathrm{th}} = \frac{(T_s + V_s)(k-1)(m+1) n_p n_s \lambda_i^2 \lambda_s c\varepsilon_0}{64\pi^2 d^2 l \xi_s}. \tag{10}$$

The signal extraction efficiency and pump depletion can be written as

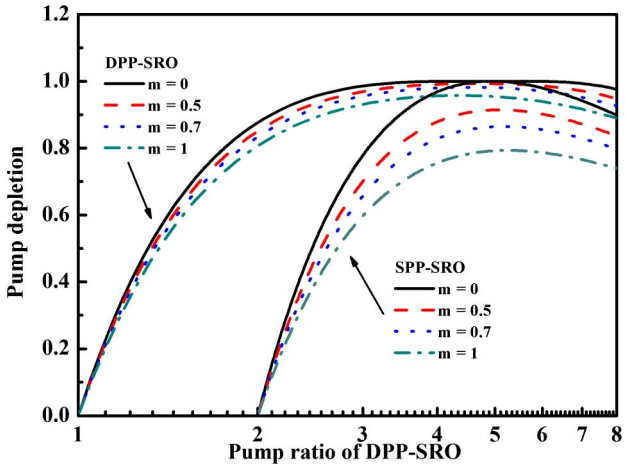

Fig. 2. Pump depletions of DPP-SRO and SPP-SRO as a function of pump ratio of DPP-SRO for different m values.

$$\eta_{p-s} = \frac{P_{s,\mathrm{out}}}{P_p} = \frac{P_s T_s}{P_p}, \tag{11}$$

$$\eta_{\mathrm{dep}} = \frac{\lambda_s (T_s + V_s) P_s}{\lambda_p P_p}. \tag{12}$$

Figure 2 shows the numerically calculated pump depletions of a DPP-SRO and SPP-SRO [20] as functions of pump ratio for different m values using the following parameters: $\varepsilon_0 = 8.854 \times 10^{-12}$ As/(Vm), $c = 3.0 \times 10^8$ m/s, $d = 9.5$ pm/V, $l = 30$ mm, $\lambda_p = 1.064$ μm, $\lambda_s = 1.56$ μm, $\lambda_i = 3.346$ μm, $n_p = 2.13$, $n_s = 2.14$, $n_i = 2.16$, $V_s = 1.4\%$. The value of V_s is determined by fitting the experiment data with the theoretical prediction from Eq. (9). According to the calculation results, the pump threshold of the DPP-SRO is half of that of the SPP-SRO. For the comparison of these two configurations, Fig. 2 is plotted using the pump ratio of the DPP-SRO as the horizontal ordinate. It refers that the value of 2 in the horizontal ordinate is corresponding to 1 of the pump ratio of the SPP-SRO. It can be seen, when $m = 0$ (i.e., in the condition of the plane-wave approximation), 100% pump depletions of the DPP-SRO and SPP-SRO can be obtained at the pump ratio of $\pi^2/2$ and $(\pi/2)^2$, respectively. When $m \neq 0$ (i.e., in the condition of the collimated Gaussian beam approximation), the pump depletions decrease with increasing m, and the pump depletion of the DPP-SRO is larger than that of the SPP-SRO at the same m. The maximum pump depletion of 98% happens at the pump ratio of about 4.5 for the DPP-SRO with $m = 0.7$.

3. EXPERIMENTAL SETUP

The experimental setup of the DPP-SRO based on PPLN is schematized in Fig. 3. The pump source is a homemade stable cw single-frequency Nd:YVO_4 laser at 1.064 μm [21] with the maximum output of 18 W and mode-hop-free operation. The DPP-SRO is a linear cavity comprising two concave mirrors of radius of curvature of 26 mm. The input coupler (M3) has high reflectivity ($R > 99.8\%$) over 1.5–1.65 μm and high transmission ($T > 95\%$) at 1.064 μm. The output coupler (M4) has

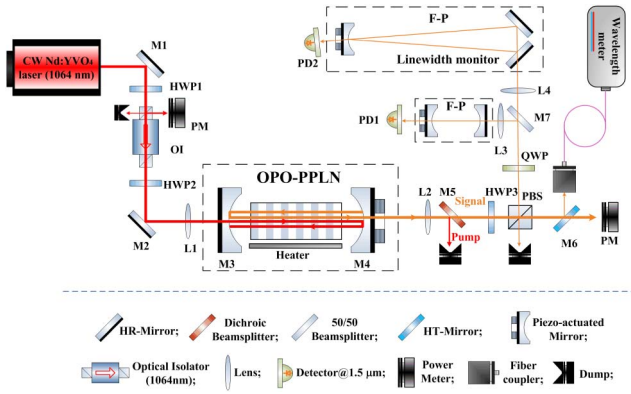

Fig. 3. Experimental setup of the DPP-SRO based on PPLN.

high reflectivity ($R > 99.9\%$) at 1.064 μm to realize the DPP scheme, and partial transmission over 1.5–1.65 μm to extract the signal. Note that the host material of the couplers is BK7 glass, which is not transparent for the light at the wavelength around 3.3 μm, the idler is not extracted from the SRO in our experiment. The powers were measured by a power meter (Model: LabMax-TOP, Coherent), while the longitudinal mode of signal was monitored using a scanning confocal Fabry–Perot (F-P) interferometer with free spectral range (FSR) of 750 MHz and finesse of 500. The wavelength of signal was measured by a wavelength meter with a resolution of 0.1 pm (Model: WS/6-771, HighFinesse).

The nonlinear crystal is a 30-mm-long PPLN crystal with a poling period of 29.8 μm that is housed in a copper oven and temperature controlled by a homemade temperature controller with an accuracy of 0.004°C. The signal wavelength can be tuned from 1.56 to 1.59 μm when PPLN temperature is controlled from 120°C to 180°C. During our experiments, the PPLN temperature was controlled at 120°C to extract the signal at 1.56 μm. The SRO cavity length was set as 64 mm. Hence the waist radii of pump and signal mode at the center of the PPLN crystal are estimated, using the ABCD-matrix method for a Gaussian beam, to be 48.5 and 59.5 μm, respectively. The pump beam was focused via a lens (L1) to a spot with radius of about 49 μm at the center of the PPLN crystal; the mode match of pump was achieved and the mode overlap between pump beam and signal mode $m = 0.68$.

4. RESULTS AND DISCUSSION

Figure 4 shows the experimental results and theoretical prediction of the extracted signal power versus pump power under different output couplers. It can be seen the pump thresholds are 2.8, 3.7, and 5.5 W at the output coupler transmissions of 1.8%, 2.5%, and 4.0%, respectively. The best SRO performance was achieved when the 2.5% output coupler is used. 6.2 W of signal at 1.56 μm was obtained at pump power of 14.5 W with 42.8% signal extraction efficiency, and the SRO could keep stable single-longitudinal-mode operation among the whole pump range. The calculated results are in good agreement with the experimental data when the pump power is lower than 10 W, but the experimental results deviate from the theoretical prediction gradually for the pump power

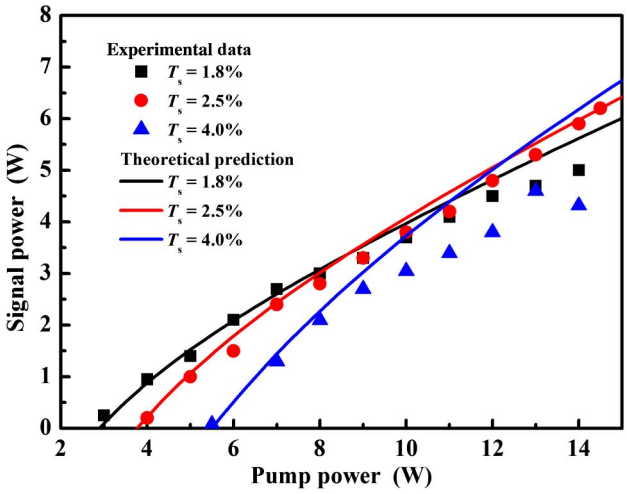

Fig. 4. Extracted signal power as a function of pump power.

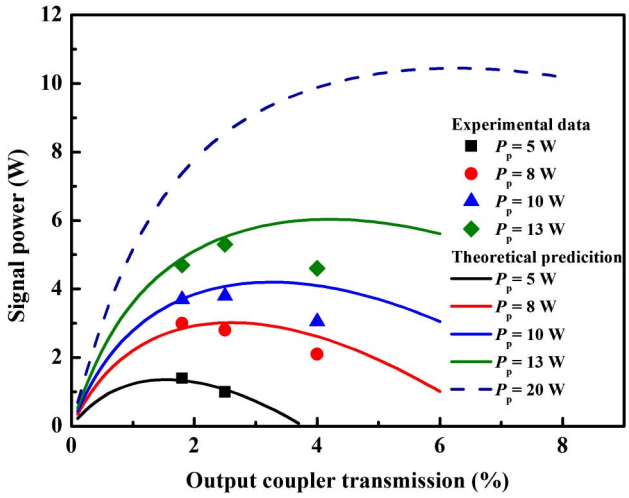

Fig. 6. Signal power as a function of output coupler transmission.

above 10 W. This behavior can be understood when one notices that there exists serious thermal effects of nonlinear crystal under high pump intensity. In particular, when the 1.8% output coupler was employed, mode hops of signal were observed frequently for the pump power above 13 W. Moreover, we also noticed that when the 4.0% output coupler was used, the coating of this mirror was damaged at pump power of 14 W, and the signal power dropped. Since the host material of the output coupler is BK7 glass, the coating damage may be due to the strong absorption of idler power.

The experimental results of pump depletion were obtained using the measured pump power and reflected pump power, as shown in Fig. 5. The black curve is the theoretical prediction using Eq. (12) and the parameter $m = 0.68$. It can be seen, the maximum measured pump depletion is 81.5% at pump ratio of 2.5 and output coupler of 1.8% that is near to the calculated result. When the optimum output coupler of 2.5% was used, the maximum measured pump depletion of 78% was achieved at pump ratio of 3.7. However, we find a great discrepancy between the experimental data and the calculation results at high pump powers. This can be explained by the fact that the value of parameters in the calculation is chosen according to the cold SRO cavity.

Figure 6 shows the dependence of signal power on output coupler transmission at different pump powers. At the pump power of 13 W, the optimum transmission of the output coupler is 2.5% in the experiment, but that is 4.2% from the calculation. Maybe we could get more signal power using the 4% output coupler if the coating was not damaged in the experiment. Anyway, the experimental results and theoretical prediction are still helpful for the optimization of the DPP-SRO. For example, the optimum output coupler should be 6.3% for the pump power of 20 W, and the corresponding signal power is 10.4 W, as shown in Fig. 6.

To understand the behavior of the DPP-SRO in detail, the signal output characteristics, such as linewidth, frequency, and power stabilities, were investigated at the signal power of 6 W. The linewidth of the signal was measured using a scanning F-P interferometer with a FSR of 75 MHz and a finesse of 1200, and recorded by a digital storage oscilloscope (Model: DPO 4054, Tektronix). As shown in Fig. 7, there was only a single

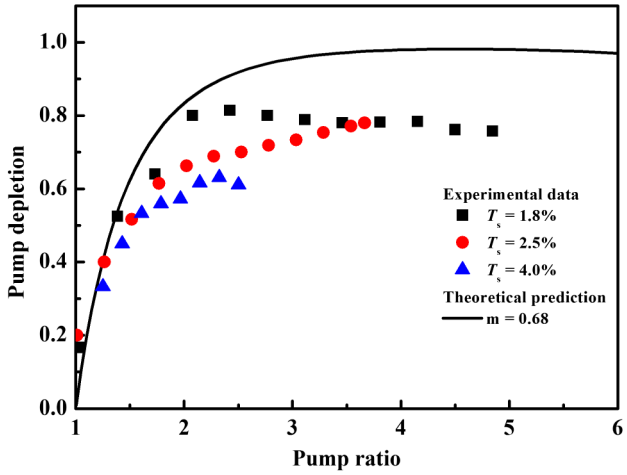

Fig. 5. Pump depletion as a function of pump ratio.

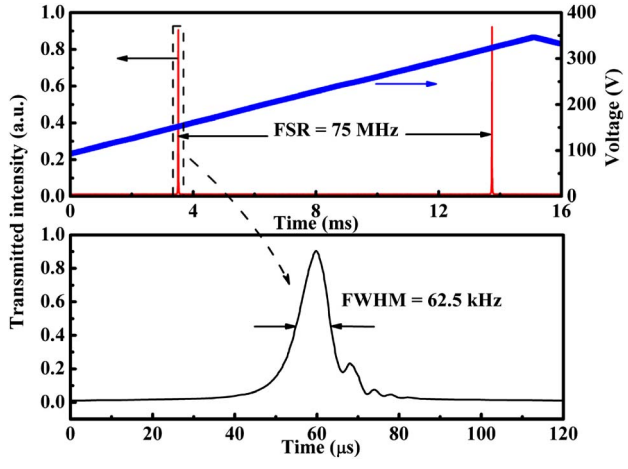

Fig. 7. Transmitted intensity from the high finesse F-P interferometer.

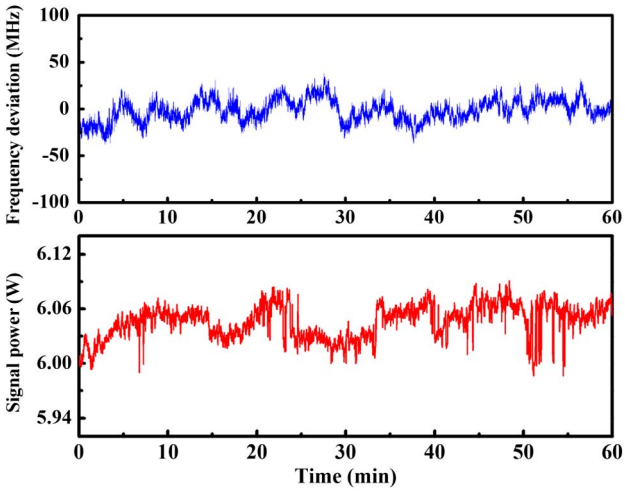

Fig. 8. Measured frequency and power stabilities of signal.

longitudinal mode, and the instantaneous linewidth was measured to be 62.5 kHz, which was limited by the resolution of the F-P interferometer.

The long-term frequency stability of the signal was measured using the wavelength meter and monitored by the scanning F-P interferometer. The frequency drift is shown in Fig. 8, together with a recording of the signal power that was measured by the power meter. Over a period of 1 h, the measured frequency deviation from the center frequency is less than ±40 MHz and the measured peak-to-peak power fluctuation is less than ±0.9%. Since the FSR of the SRO cavity is 1.5 GHz, the SRO is confirmed to be mode-hop-free operated from the data. With the help of the homemade stable single-frequency Nd:YVO_4 laser at 1.064 μm as the pump source and the excellent temperature controller to control the PPLN temperature, the excellent performance of the DPP-SRO was achieved without adding any additional elements in the cavity or active stabilization.

5. CONCLUSION

We have theoretically investigated DPP-SRO with an extension of the theories developed in [20] that is used to guide the design and optimization of a PPLN-based DPP-SRO. After optimizing the signal output using different output couplers, the excellent performance such as low pump threshold, high signal output power, and narrow linewidth were realized simultaneously at 2.5% output coupler. The pump threshold was as low as 3.7 W, and 6.2 W of signal at 1.56 μm with the linewidth of 62.5 kHz was obtained at pump power of 14.5 W. Moreover, with the help of the homemade stable pump source and the excellent temperature controller, the DPP-SRO can be mode-hop-free operated stably without adding any additional elements in the cavity or active stabilization. The measured signal frequency drift and peak-to-peak power fluctuation are less than ±40 MHz and ±0.9% in a given 1 h, respectively. This kind of stable, high-power, narrow linewidth single-frequency laser at 1.56 μm can be used to produce the continuous variable quantum entanglement at a telecommunication wavelength.

National Major Scientific Equipment Developed Project of China (2011YQ030127); National Natural Science Foundation of China (11204167, 61227015, 61405109).

REFERENCES

1. P. Groß, I. D. Lindsay, C. J. Nittmann, T. Bauer, J. Bartschke, U. Warring, A. Fischer, A. Kellerbauer, and K.-J. Boller, "Frequency control of 1163 nm singly resonant OPO based on MgO:PPLN," Opt. Lett. **35**, 820–822 (2010).
2. E. V. Kovalchuk, D. Dekorsy, A. I. Lvovsky, C. Braxmaier, J. Mlynek, A. Peters, and S. Schiller, "High-resolution Doppler-free molecular spectroscopy with a continuous-wave optical parametric oscillator," Opt. Lett. **26**, 1430–1432 (2001).
3. S. M. Cristescu, S. T. Persijn, S. Te Lintel Hekkert, and F. J. M. Harren, "Laser-based systems for trace gas detection in life sciences," Appl. Phys. B **92**, 343–349 (2008).
4. T. Eberle, V. Handchen, J. Duhme, T. Franz, F. Furrer, R. Schnabel, and R. F. Werner, "Gaussian entanglement for quantum key distribution from a single-mode squeezing source," New J. Phys. **15**, 053049 (2013).
5. V. C. Usenko and R. Filip, "Squeezed-state quantum key distribution upon imperfect reconciliation," New J. Phys. **13**, 113007 (2011).
6. J. X. Feng, X. T. Tian, Y. M. Li, and K. S. Zhang, "Generation of a squeezing vacuum at a telecommunication wavelength with periodically poled $LiNbO_3$," Appl. Phys. Lett. **92**, 221102 (2008).
7. T. Eberle, V. Händchen, and R. Schnabel, "Stable control of 10 dB two-mode squeezed vacuum states of light," Opt. Express **21**, 11546–11553 (2013).
8. J. X. Feng, Y. M. Li, X. T. Tian, J. L. Liu, and K. S. Zhang, "Noise suppression, linewidth narrowing of a master oscillator power amplifier at 1.56 μm and the second harmonic generation output at 780 nm," Opt. Express **16**, 11871–11877 (2008).
9. S. Taccheo, G. Sorbello, P. Laporta, G. Karlsson, and F. Laurell, "230-mW diode-pumped single-frequency Er:Yb laser at 1.5 μm," IEEE Photon. Technol. Lett. **13**, 19–21 (2001).
10. Y. J. Li, J. X. Feng, P. Li, K. S. Zhang, Y. J. Chen, Y. F. Lin, and Y. D. Huang, "400 mW low noise continuous-wave single-frequency Er, Yb:$YAl_3(BO_3)_4$ laser at 1.55 μm," Opt. Express **21**, 6082–6090 (2013).
11. P. Zeil, N. Thilmann, V. Pasiskevicius, and F. Laurell, "High-power, single-frequency, continuous-wave optical parametric oscillator employing a variable reflectivity volume Bragg gating," Opt. Express **22**, 29907–29913 (2014).
12. S. T. Lin, Y. Y. Lin, Y. C. Huang, A. C. Chiang, and J. T. Shy, "Observation of thermal-induced optical guiding and bistability in a mid-IR continuous wave, singly resonant optical parametric oscillator," Opt. Lett. **33**, 2338–2340 (2008).
13. A. Henderson and R. Stafford, "Spectral broadening and stimulated Raman conversion in a continuous-wave optical parametric oscillator," Opt. Lett. **32**, 1281–1283 (2007).
14. S. C. Kumar, R. Das, G. K. Samanta, and M. Ebrahim-Zadeh, "Optimally-output-coupled, 17.5 W, fiber-laser-pumped continuous-wave optical parametric oscillator," Appl. Phys. B **102**, 31–35 (2011).
15. D. Pabœuf, O. Mhibik, F. Bretenaker, and C. Drag, "Optimization of the resonant wave output coupling of a singly resonant optical parametric oscillator using an intracavity plate," Appl. Phys. B **108**, 289–293 (2012).
16. R. Sowade, I. Breunig, J. Kiessling, and K. Buse, "Influence of the pump threshold on the single-frequency output power of singly resonant optical parametric oscillators," Appl. Phys. B **96**, 25–28 (2009).
17. M. Vainio, J. Peltola, S. Persijn, F. J. M. Harren, and L. Halonen, "Thermal effects in singly resonant continuous-wave optical parametric oscillator," Appl. Phys. B **94**, 411–427 (2009).

18. I.-H. Bae, H. S. Moon, S. Zaske, C. Becher, S. K. Kim, S.-N. Park, and D.-H. Lee, "Low-threshold singly-resonant continuous-wave optical parametric oscillator based on MgO-doped PPLN," Appl. Phys. B **103**, 311–319 (2011).
19. J. E. Bjorkholm, A. Ashkin, and R. G. Smith, "Improvement of optical parametric oscillators by non-resonant pump reflection," IEEE J. Quantum Electron. **QE-6**, 797–799 (1970).
20. S. Guha, "Focusing dependence of the efficiency of a singly resonant optical parametric oscillator," Appl. Phys. B **66**, 663–675 (1998).
21. Q. Liu, J. L. Liu, Y. C. Jiao, J. X. Feng, and K. S. Zhang, "A stable 22-W low-noise continuous-wave single-frequency Nd:YVO_4 laser at 1.06 μm directly pumped by a laser diode," Chin. Phys. Lett. **29**, 054205 (2012).